

Antibiotic detoxification from synthetic and real effluents using a novel MTAB surfactant-montmorillonite (organoclay) sorbent†

Cite this: *RSC Adv.*, 2014, 4, 16298

Merry Anggraini,^a Alfin Kurniawan,^a Lu Ki Ong,^a Mario A. Martin,^a Jhy-Chern Liu,^b Felycia E. Soetaredjo,^a Nani Indraswati^a and Suryadi Ismadji*^a

The growing threat of antibiotic-resistant bacteria to public health has raised interest in the proper treatment of discharged pharmaceutical wastewater before entering surface waters. In this study, adsorption was highlighted as a low cost and effective pathway to remove amoxicillin and ampicillin from aqueous solutions. Montmorillonite (Na-MMT) and myristyltrimethylammonium (MTA)-intercalated montmorillonite (O-MMT) were employed as the adsorbing solids. Static adsorption experiments were performed at three temperatures (303.15 K, 313.15 K and 323.15 K) for single antibiotic systems. The adsorption isotherm curves at all temperatures exhibited an L2-type isotherm. The Freundlich and Langmuir models were applied to analyze single adsorption isotherm data. The maximum sorption capacity of 0.124–0.133 mmol g⁻¹ for amoxicillin and 0.143–0.157 mmol g⁻¹ for ampicillin was estimated for O-MMT sorbent from Langmuir fitting. A modified extended-Langmuir model with the inclusion of surface coverage (θ) was proposed for analysis of binary adsorption isotherm data. The fitness of the modified extended-Langmuir model was superior to the original model. Batch adsorption tests on real pharmaceutical wastewater demonstrated the feasibility of the O-MMT sorbent for practical applications.

Received 13th January 2014
Accepted 20th March 2014

DOI: 10.1039/c4ra00328d

www.rsc.org/advances

Introduction

Currently, a large group of antibiotics is available in the market and they have been proven to be powerful drugs to treat various bacterial infections, from minor to life-threatening ones. Antibiotics are generally produced by or derived from microorganisms such as fungi or bacteria and they can also be chemically synthesized and particular examples are penicillins, cephalosporins, macrolides, rifamycins, sulfonamides, chloramphenicol, tetracyclines and aminoglycosides. Of particular interest are penicillin groups including amoxicillin and ampicillin. Amoxicillin is a moderate-spectrum of β -lactam antibiotics and is usually the drug of choice within penicillin groups due to its better absorptivity, following oral administration than other β -lactam antibiotics. Amoxicillin is widely used in the treatment of a number of bacterial infections include pneumonia, bronchitis, laryngitis, gonorrhoea, skin and urinary tract infections.¹ Ampicillin is also a β -lactam antibiotic, part of the

aminopenicillin family, which is closely related to amoxicillin in terms of spectrum and activity level.² Both amoxicillin and ampicillin work in a similar manner against Gram Positive and Gram Negative bacteria by interfering cell wall synthesis so that the human antibodies can penetrate and remove them.² In spite of its usefulness and valuable contributions in human therapy, antibiotic-resistant bacteria are the today's most pressing clinical and public health concerns that continue to grow due to abuse and overuse of antibiotics. This leads to consequent treatment complications and increased healthcare costs because the target bacteria are becoming more resistant to the exposure of therapeutic levels of an antibiotic.

The dissemination of antibiotics in natural environments (*e.g.*, lakes and streams) may come from various sources, such as human and animal excretion, agriculture, aquaculture and livestock farming, hospital sewage sludge and diverse industrial routes.³ The relative concentrations of antibiotics in the industrial effluents are several order of magnitude higher than those released from veterinary and hospital sources.³ Although most of pharmaceutical products administered are particularly designed to have a short half-life, some antimicrobials like tetracycline, erythromycin, sulfamethoxazole and penicilloyl groups are persistence and poorly metabolized hence they are only partially eliminated in the sewage treatment plants. The enrichment of antibiotic residues and their transformed products into receiving waters is worrying as it can impact the

^aDepartment of Chemical Engineering, Widya Mandala Surabaya Catholic University, Kalijudan 37, Surabaya 60114, Indonesia. E-mail: suryadiismadji@yahoo.com; Fax: +62 31 389 1267; Tel: +62 31 389 1264

^bDepartment of Chemical Engineering, National Taiwan University of Science and Technology, No. 43, Sec. 4, Keelung Rd., Taipei City 106, Taiwan, Republic of China

† Electronic supplementary information (ESI) available. See DOI: 10.1039/c4ra00328d

structure and activity of microbiota, spreading of antibiotic-resistant genes to pathogenic bacteria strains that can reach humans through food chains and ultimately in the water reuse scenario.^{4–6}

Several treatment methods have been developed so far for purification of antibiotic-bearing effluents such as aerobic and anaerobic biological treatments,^{7,8} advanced chemical oxidation,^{9–11} membrane separation,¹² chlorination,¹³ photocatalysis,^{14–16} electro-oxidation,¹⁷ and adsorption.^{18–21} Amongst them, adsorption is considered as the most reliable method for removal of toxic micropollutants from municipal water and wastewater. Regardless of the adsorbent material and system design, adsorption process is generally simple, adaptable, economically viable and highly effective across a wide range of concentrations, highlighting its advantages over other technologies. The treatment of water and wastewater containing antibiotics by adsorption is the key to modulating the extent of environmental occurrence, transport and fate of this micropollutant.

Clays and clay minerals have found potential applications for sustaining the environment because they exhibit large adsorption capacity, excellent mechanical and chemical stability, cheap and readily obtained in large quantities. So, efforts toward their applications as a sorbent to abate antibiotics from water and wastewater have been stimulated. Over the past few years, a progressing research on the removal of antibiotics using clays or clay minerals can be found in literatures.^{18–21} In most, if not all, of these studies, single adsorption systems are emphasized and only limited studies dedicate to investigate binary or multi-component systems. In the real pharmaceutical sewage treatment units, two or more unmetabolized antibiotics may co-exist, thus it is necessary to study binary or multicomponent adsorption equilibria and thermodynamics for effective design and optimization of antibiotic/clay wastewater treatment systems. To fill this gap, the goals of this study are (1) to synthesize a novel organoclay sorbent and (2) to evaluate the performance of pristine and as-synthesized organoclay to remove amoxicillin and ampicillin from single and binary (two components) aqueous systems. As far as we are aware, this is the first study demonstrating binary adsorption of amoxicillin and ampicillin using pristine and myristyltrimethylammonium cation-intercalated (organo) montmorillonite with special attentions to adsorption equilibria and thermodynamic aspects. We propose a modification on the extended-Langmuir model by introducing surface coverage for analyzing binary adsorption equilibrium data. Ultimately, batch adsorption tests on real pharmaceutical wastewater are demonstrated, along with regenerability evaluation of the clay sorbent.

Experimental section

Chemicals

Antibiotics used in this study (*i.e.*, amoxicillin trihydrate and ampicillin trihydrate) were kindly provided by a local pharmaceutical industry with minimum purity of 97% and 95%, respectively. The molecular structure and some specific information about these compounds include their environmental persistence data^{22,23} are presented in Table 1. Analytical-grade

chemicals include myristyltrimethylammonium bromide (MTAB) cationic surfactant (99%), hydrogen peroxide solution (30%), sodium chloride (99.5%), hydrochloric acid (37%), silver nitrate (99.8%) and potassium hydroxide (85%) were purchased from Sigma-Aldrich, Singapore and used as-supplied. Double distilled water (DDW) was used throughout the experiments.

Preparation of adsorbent materials

Montmorillonite lumps as the starting material were collected from one of mining sites located at Pacitan town, East Java. After the collection, the solid was repeatedly washed with tap water to remove coarse particles and water-soluble impurities. Then, the solid was dispersed in dilute hydrogen peroxide solution with a solid/solution ratio of 1 : 10 (w/v) and the suspension was aged for 2 h under mechanical stirring at 500 rpm. The solid was washed with double distilled water and 0.1 N NaOH solution alternately until the pH of the washing solution was near-neutral. The clay material was oven-dried at 383.15 K and stored in an airtight plastic bag for further characterizations. The mineralogical analysis of clay material was conducted based on the size fractionations method²⁴ and the results are: 72% smectite, 4% quartz, 12% feldspar, 8% calcite, 3% anatase and 1% others.

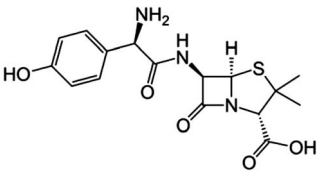
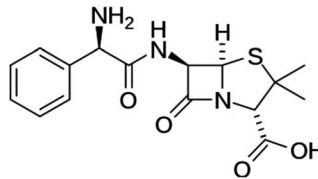
To enhance the monoionic nature of clay, fifty grams of clay was treated with 250 mL 1 N NaCl solution (five cycles stirred at 500 rpm for an hour in each cycle) and washed until negative reaction of chloride ions with silver nitrate was obtained. The resulting clay (denoted as Na-MMT) was oven-dried at 373.15 K for 24 h, pulverized and screened with 100/120 sieves to obtain size fractions of 0.125–0.150 mm. The cation exchange capacity (CEC) of Na-MMT was 74.2 m eq./100 g of clay, as measured by methylene blue index following ASTM C837-99 test method. The metal oxide compositions of Na-MMT were analyzed using a PANalytical MiniPal QC energy dispersive X-ray fluorescence (EDXRF) spectrometer and the results are shown as follows: SiO₂ of 61.28%; Al₂O₃ of 18.33%; Na₂O of 2.47%, K₂O of 1.75%, MgO of 2.16%, CaO of 1.59%, MnO of 0.27%, Fe₂O₃ of 3.35%, and TiO₂ of 0.08%.

The preparation procedure of organo-montmorillonite (designated as O-MMT) was described as follows: 10 g Na-MMT was dispersed in 100 mL MTAB solution with a surfactant concentration equivalent to 1.5 times of the CEC of clay. The suspension was aged for 1 h under stirring at 500 rpm. Then, it was placed in an Inetron WDS900DSL23-2 microwave oven and irradiated over 5 min at a frequency of 2.45 GHz and an output power of 500 W. The resulting solid was washed with double distilled water several times until it was free from bromide anions (tested by titration with 0.1 M AgNO₃ solution). The product was dried in an air-circulating oven at 383.15 K to constant weight, pulverized and sieved. The CEC of O-MMT was 14.9 m eq./100 g of clay according to methylene blue adsorption index.

Characterizations of adsorbent materials

Scanning electron microscopy (SEM) was performed to probe the microtopography and surface texture of the adsorbents. The scanning was conducted on a JEOL JSM-6390 field emission

Table 1 Molecular structure and some specific information about amoxicillin and ampicillin

	Amoxicillin	Ampicillin
Molecular structure		
Physical state	White to off-white solid	White to off-white solid
Molar mass (g mol ⁻¹)	365.4	349.4
Chemical formula	C ₁₆ H ₁₉ N ₃ O ₅ S	C ₁₆ H ₁₉ N ₃ O ₄ S
Water solubility, 25 °C (g L ⁻¹)	3.43	10.1
pK _a	2.4 (carboxylic) 7.4 (amine) 9.6 (phenol)	2.7 (carboxylic), 7.3 (amine)
Environmental persistence data		
Photodegradation rate (s ⁻¹)		
Direct ^a	5.24 × 10 ⁻⁷	Not available
Hydrolysis rate (s ⁻¹) ^b	4.45 × 10 ⁻⁷	2.15 × 10 ⁻⁷

^a Direct photodegradation at pH 7 using a solar simulator system. ^b Hydrolysis at pH 7 and room temperature (298.15 K); the hydrolysis rate constants correspond to half-lives of 18 d for amoxicillin and 36 d for ampicillin.

SEM at an accelerating voltage of 20 kV. Surface characterizations were conducted by physical adsorption-desorption isotherms of N₂ at 77.15 K, on a Micromeritics ASAP 2010 automated sorptometer. The samples were vacuum-outgassed under a flow of pure helium at 10⁻³ Torr and 473.15 K for 24 h. The specific surface area, micropore volume (*V*_{mic}) and external (mesoporous) surface area (*S*_{ext}) was determined from the adsorption branches applying the Brunauer-Emmett-Teller (BET) and *t*-plot method, respectively. The pore size distribution was derived from desorption data by means of Barrett-Joyner-Halenda (BJH) method. Total pore volume (*V*_T) was estimated from the volume of gas adsorbed at a relative pressure (*p/p*^o) of 0.99.

The pH of point of zero charge (pH_{pzc}) was determined by pH-drift technique following Yang *et al.*²⁵ method. Briefly, a solution of 0.005 M CaCl₂ was boiled to remove dissolved CO₂ and then cooled to room temperature. A 20 mL aliquot of the solution was poured into a series of capped vials. The pH was adjusted by adding 0.5 M HCl or 0.5 M NaOH solution to a value between 2 and 11. A known amount of Na-MMT or O-MMT (±0.05 g) was added and the suspension was equilibrated for 24 h. The final pH was measured using a SevenEasy™ digital pH-meter (Model S20, Mettler Toledo) and plotted against the initial pH. The pH at which the curve of pH_{final} versus pH_{initial} crosses the line pH_{initial} = pH_{final} is marked as pH_{pzc}. The results are 5.82 for pH_{pzc} of Na-MMT and 7.18 for pH_{pzc} of O-MMT.

Thermal decomposition analysis was performed on a Mettler-Toledo TGA/DSC 1 thermogravimetric analyzer. Approximately 10 mg of the samples was spread uniformly at the bottom of alumina crucible. The temperature of furnace was programmed to rise from room temperature to a final temperature of 1123.15 K at 20 K min⁻¹ in a dynamic high-purity flowing N₂ of 100 mL min⁻¹. The elemental contents of Na-MMT and O-MMT

materials were determined using an automated CHNS/O elemental analyzer (Model 2400-II, PerkinElmer). FT-IR analysis was carried out on a Shimadzu FTIR 8400S spectrometer using KBr disk technique. The spectra data were collected by accumulating 200 scans over wavenumber range of 4000–500 cm⁻¹ in the transmission mode at a spectral resolution of 4 cm⁻¹. Data processing includes baseline adjustment, normalization and spectral smoothing was performed using IRsolution software (Version 1.21). The mineralogical compositions of the solids were analyzed using a Philips PANalytical X'Pert X-ray diffractometer. The powder diffractograms of the specimens were acquired at 40 kV and 30 mA in the range of 2-theta angles of 2–70° with a scanning speed of 1°/min. The radiation source was Ni-filtered Cu Kα₁ (λ = 0.15405 nm).

Batch adsorption experiments – single solute systems

Fresh antibiotic effluents were prepared by dissolving 0.3 g amoxicillin or ampicillin into 1 L deionized water to give an initial concentration of 0.80 mmol L⁻¹ for amoxicillin and 0.82 mmol L⁻¹ for ampicillin. For the adsorption equilibrium experiments, the stock effluents of amoxicillin or ampicillin were poured into a series of stoppered conical flasks (each of 100 mL) containing Na-MMT or O-MMT with varying doses (0.1–1 g). The flasks were wrapped with aluminium foil to eliminate light interference. Then, the flasks were placed in a thermostated reciprocal shaker and shaken at 100 rpm for 24 h. Preliminary experiments indicated that 24 h provided sufficient time to reach equilibrium. The system temperature was held constant at 303.15 K, 313.15 K and 323.15 K by a built-in PID-type temperature controller. After equilibration, the clay suspension was centrifuged at 3000 rpm for 10 min and the supernatant was taken for analysis. The residual concentration of solute was quantified by a double beam UV-Vis spectrophotometer at a

detection wavelength of 252.2 nm for amoxicillin and 245.8 nm for ampicillin. The calibration curves were prepared from a set of five standard solutions with concentration range of 50–300 mg L⁻¹. Prior to spectrophotometric measurements, all supernatants were filtered through a 0.45 μm syringe filter. The amount of solute adsorbed per unit mass of adsorbent at equilibrium (q_e , mmol g⁻¹) was determined by the following equation:

$$q_e = \frac{C_0 - C_e}{m} V \quad (1)$$

where C_0 and C_e are the initial and equilibrium concentrations of solute in the liquid phase (mmol L⁻¹), respectively, m is the mass of adsorbent (g) and V is the volume of solution (L). For the pH adsorption edge experiments, the suspension pH was varied from 2 to 11 and adjustment was made by adding 1 N HCl or 1 N KOH solutions. All adsorption runs were replicated twice with averages used as the results.

Batch adsorption experiments – binary solute systems

For the binary adsorption experiments, three synthetic effluents containing amoxicillin and ampicillin were prepared (Table S1 of the ESI†). Adsorption isotherm experiments were performed in a closed batch system by equilibrating the synthetic effluents containing a known amount of O-MMT on a reciprocal shaker for 24 h at room temperature. The initial pH of all effluents ranged between 6 and 7. The equilibrium concentration of remaining antibiotics was determined spectrophotometrically in a multi-component quantitation mode at two measurement wavelengths of 245.8 nm and 252.2 nm. Five mixed samples with pure amoxicillin and ampicillin standards were made to construct the calibration curve. The following mathematical formula was used to calculate the equilibrium amount of solutes i and j in the adsorbed phase:

$$q_{e,i/j} = \frac{(C_{0,i/j} - C_{e,i/j})}{m} \times V \quad (2)$$

where $q_{e,i}$ and $q_{e,j}$ are the equilibrium loading of solutes i and j in the solid phase (mmol g⁻¹), C_0 and C_e refer to the initial and equilibrium concentrations of solute in the solution (mmol L⁻¹), m is the mass of O-MMT used (g) and V is the volume of the effluents (L).

Results and discussion

Textural properties and surface chemistry of Na-MMT and O-MMT materials

The electron micrographs of Na-MMT and O-MMT are shown in Fig. 1. SEM analysis confirmed that Na-MMT and O-MMT are both crystalline solids of micrometer size. The lump alike morphology of Na-MMT with smooth surface characteristic is clearly seen from Fig. 1a. In comparison, the SEM image of O-MMT displays the agglomerated sheet like morphological feature and surface roughness (Fig. 1b). N₂ adsorption-desorption isotherms (Fig. S1 of the ESI†) ascertain that both clay sorbents are highly mesoporous with mixed micro- and meso-sized pores. The characteristic type H4 hysteresis loop observed in the relative pressure range of 0.4–0.6 is the

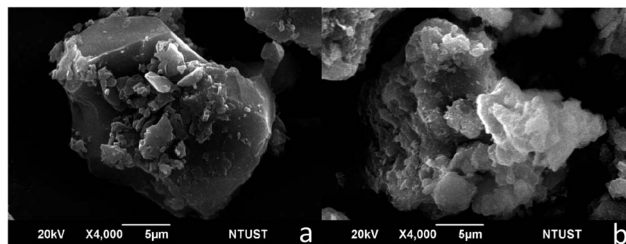


Fig. 1 SEM images of Na-MMT (a) and O-MMT (b).

indication of an adsorption phenomenon of gases typical for complex micro-mesoporous solids, which include micropores filling, pore condensation and cavitation-induced evaporation mechanisms.²⁶ The BET specific surface area of Na-MMT was 122.2 m² g⁻¹ and this value dramatically fell to 65.8 m² g⁻¹ of O-MMT. Similarly, total pore volume of Na-MMT was 0.11 cm³ g⁻¹ while that of O-MMT was 0.06 cm³ g⁻¹ (Table S2 of the ESI†). The decreased BET specific surface area and pore volume revealed that some interior adsorption sites became inaccessible by N₂ molecules due to the blocking of large surfactant cations within the pores. The pore size distribution curves (inset Fig. S1†) support N₂ adsorption-desorption results that high percentage of mesopores with a diameter about 3–4 nm exist in Na-MMT and O-MMT. Furthermore, a notable distribution of pore sizes outside the range of 3–4 nm was observed in O-MMT, likely due to the surfactant cations loading into the interparticle pores within the ‘house-of-cards’ structure that enlarge the corresponding pore size. This is consistent with other studies dealing with organoclay preparation employing long alkyl-chain cationic surfactants.^{27–29} Confirmation of the organification of Na-MMT was also shown from elemental analysis results in the ESI Table S3.† In this table, it can be seen that O-MMT contains about 0.83 wt% N and 12.1 wt% C (the C/N ratio is 14.58) where the presence of carbon and nitrogen atoms in Na-MMT is not observed. Based on the carbon and nitrogen contents, it can be estimated that each gram of clay contains 0.59 mmol of intercalated C14-trimethylammonium cations.

Thermal gravimetric analysis was used to examine the weight loss arising from organic content and the related degradation mechanisms. The TGA curves in the ESI Fig. S2† show that the weight loss by about 7% below 150 °C corresponds to the loss of surface water and water associated with Na-MMT micropore structure. Between 200 °C and 400 °C, about 0.0063 g H₂O per g clay was lost, which might be attributed to desorption of water from the interlayer space. Irreversible dehydroxylation of the layered silicate structure takes place in the temperature range of 600–700 °C. The weight change of the clay could be neglected above 700 °C. The presence of organic moieties increases the number of decomposition steps for organoclay. As illustrated in Fig. S2,† the TGA profile of O-MMT indicates four weight-loss steps: (I) the loss of water (dehydration) that occurs at 110 °C and ends at 150 °C; (II) decomposition of the bonded structure of organic modifier in the interlayer space at 200–300 °C; (III) dehydroxylation of the silicate layers around 600 °C and proceeds till around 700 °C and (IV) further decomposition of the organic surfactant at

720–800 °C. The thermogram pattern of bare MTAB indicates the weight loss at 110 °C resulted from dehydration, followed by structural degradation that occurs at 250–400 °C. Finally, the maximum decomposition takes place around 600 °C due to the incomplete oxidation of the organic moieties under N₂ atmosphere.

The spectral characteristics of Na-MMT and O-MMT are displayed in the ESI Fig. S3.† Several infrared absorption bands of Na-MMT were observed at specific wavenumbers, which are the typical of montmorillonitic mineral: 3614 cm⁻¹ of O–H stretching of structural hydroxyl groups located at the surface and along the broken edges, 3342 cm⁻¹ and 1636 cm⁻¹ of stretching and bending vibrations of OH group in water molecules, 1087 cm⁻¹ of Si–O stretching, 936 cm⁻¹ of Al–Al–OH hydroxyl-bending vibration, 522 cm⁻¹ of Al–O–Si bending vibration and 475 cm⁻¹ of Si–O–Si bending vibration. The insertion of organic modifier (MTA⁺ cation) into the interlayer spacing gave rise to symmetric and asymmetric sp³ C–H stretching vibrations of methyl and methylene groups at 2900–2800 cm⁻¹ and symmetric sp³ C–H bending vibration at 1464 cm⁻¹. It can be shown that the vibrational bands correspond to Si–O stretching, Al–Al–OH bending, Al–O–Si bending and Si–O–Si bending between Na-MMT and O-MMT are essentially identical. This suggests that the unit-cell framework of montmorillonite mineral (tetrahedral-octahedral-tetrahedral layered sheets) remains intact during microwave irradiation. On the other hand, the absorption intensities of stretching and bending vibrations of hydroxyl group at ~3400 cm⁻¹ and ~1600 cm⁻¹ dropped, which might be attributed to the removal of adsorbed water molecules from the clay lattice.

X-ray diffractograms of Na-MMT and O-MMT are given in the ESI Fig. S4.† Here, the XRD pattern of MMT lump was not shown due to its similar characteristic to that pattern of Na-MMT. A broad (001) reflection was noted at 2-theta of 6.44° for MMT lump and 6.49° for Na-MMT, characterizing the basal spacing of montmorillonite. This information suggested that the transformation of MMT lump to Na-MMT through cation exchange did no or little alteration on the mineralogical properties of clay. The occurrence of other crystalline phases such as quartz, calcite, feldspar and anatase was observed in addition to montmorillonite crystal planes and basal reflections. Semi-quantitative mineral analyses of MMT lump and Na-MMT based on XRD data showed that these clay impurities accounted for 20–22% of total crystalline phases (the purity of smectite phase was 78–80%). The intercalation of MTA⁺ cations into the montmorillonite structure leads to the expansion of basal spacing from 1.36 nm to 1.95 nm and interlayer spacing from 0.39 nm to 0.98 nm. The interlayer spacing was determined by subtracting the measured basal spacing with the unit-cell thickness of a single tetrahedral-octahedral-tetrahedral layered sheet of montmorillonite, which is 0.97 nm.³⁰ The structural conformation of the surfactant in the interlayer spacing can be interpreted by considering the magnitude of increased basal spacing and the molecular structure of intercalated surfactant cations (the thickness of polar ‘head’ and apolar ‘tail’). The loading of MTA⁺ cation, a single C14 alkyl chain trimethylammonium surfactant with a concentration of 1.5 times of the

CEC would result in the pseudotrilayer conformation; that is the alkyl chain of surfactant is packed in parallel to the plane of silicate tetrahedral sheets with interlocked-chains array.^{27,31} The equivalence exchange between Na⁺ and MTA⁺ cations also renders the clay surface to be organophilic, which is suitable to sorb organic compounds such as antibiotics.

Effects of solution pH on the adsorptive removal of amoxicillin and ampicillin

The pH is a crucial factor both towards the surface charge density of adsorbent and the ionic speciation of adsorbate in the liquid phase, which determines the effectiveness of a sorption process. The presence of acid (carboxylic) and base (amino) surface functional groups within amoxicillin and ampicillin structure contributes to the amphoteric nature of these drugs, in which these groups are ionisable following the pH changes. As shown in Table 1, amoxicillin has three acid dissociation constants of 2.4 (pK_{a1} of carboxylic), 7.4 (pK_{a2} of amine) and 9.6 (pK_{a3} of phenol) while for ampicillin, the pK_a values are 2.7 (carboxylic) and 7.3 (amine).¹⁴ Accordingly, amoxicillin species are mainly as a cation in the acidic solution (pH < 2.4), a zwitterion between pH 2.4 and 7.4 and an anion in the alkaline solution (pH > 7.4). Similarly, ampicillin exists predominantly in cationic, zwitterionic and anionic forms at pH < 2.7, 2.7 < pH < 7.3 and pH > 7.3, respectively (see Fig. S5 of the ESI†). The distribution diagrams showing the percentage of amoxicillin and ampicillin species at room temperature under different solution pHs was presented in the ESI Fig. S6.†

The influence of pH on the adsorbed amount of amoxicillin and ampicillin in single systems is given in Fig. 2. In this figure, the increasing amount of amoxicillin or ampicillin adsorbed by Na-MMT was seen with the increase of pH from 2 to 7 and then a progressive decrease on the removal percentage was encountered at pH above 7. Similar observation was reported by Moussavi *et al.* for the removal of amoxicillin from water using NH₄Cl-induced activated carbon.³² The limited uptake at low pH, particularly below pK_{a1} of amoxicillin or ampicillin was due to net repulsion between positively charged edge hydroxyl surfaces of montmorillonite crystallites (silanol and aluminol sites) and the cationic adsorbate molecules. From the speciation diagrams in Fig. S5,† it can be shown that at low pH range (pH 2–3), the cationic amoxicillin and ampicillin accounted for 84% and 86% of total species in the solution, respectively. The removal processes of amoxicillin (~24%) and ampicillin (~27%) could still take place in the acidic environment due to the dipole-induced interaction between protonated amine group and the Si-tetrahedral basal oxygen surface in addition to ion exchange between Na⁺ interlayer cations and protonated amoxicillin or ampicillin. The latter phenomenon (cation exchange) has been verified to be the sorption controlling mechanism at low pH in the studies conducted by Jiang *et al.*³³ and Wang *et al.*³⁴ for the removal of ciprofloxacin using layered manganese oxide and Ca-montmorillonite, respectively.

With the increase of pH approaching pK_{a2} of the adsorbate, the ratio of zwitterion to cation increases gradually for both antibiotics and this leads to the increase of removal percentage,

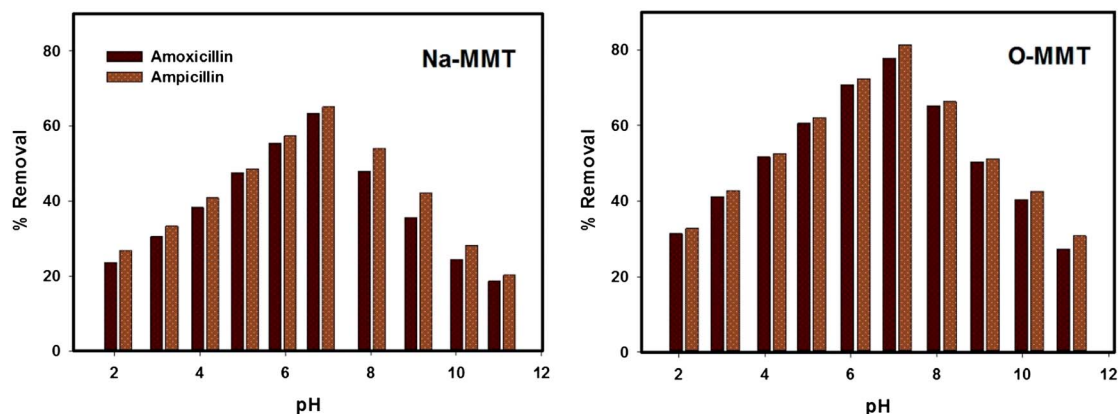


Fig. 2 Variation of pHs on the removal of amoxicillin and ampicillin in single component systems (adsorbent dosage = 1 g L⁻¹, contact time = 24 h, T = 303.15 K).

reaching the highest level of 63.5% for amoxicillin and 65.2% for ampicillin at near-neutral pH. Under this condition, the protonated amine in amoxicillin or ampicillin structure might play important for the enhanced removal process by forming electric force that attracts this cationic group to deprotonated aluminol (Al-O⁻) or silanol (Si-O⁻) edge sites. Furthermore, the concentration of H⁺ ions that compete with NH₃⁺ group for the basal oxygen surfaces diminished at elevated pH, facilitating the sorption process. The sorption of amoxicillin or ampicillin under alkaline environment is unfavorable since both antibiotics exist as an anion (attributed to the presence of conjugate bases of carboxylic acid and phenol groups) thus electrostatic repulsive force dominates. Such phenomenon was confirmed from a gradual decline on the removal percentage from 63.5% to 18.7% for amoxicillin and 65.2% to 20.3% for ampicillin as the pH rose from 7 to 11.

For the adsorption of amoxicillin or ampicillin using O-MMT, higher removal percentage was observed across the pH range studied, indicating that O-MMT has superior adsorption capacity. In the acidic solution, about 31–61% of amoxicillin and 33–62% of ampicillin was removed while the removal efficiency in highly alkaline environments (pH 10–11) ranged between 27% and 41% for amoxicillin and 31–43% for ampicillin. The highest removal percentage was obtained at pH around 7, corresponding to 77.8% removal for amoxicillin and 81.3% removal for ampicillin. It can be implied that higher adsorptive removal of O-MMT was mainly attributed to the exchange of interlayer Na⁺ cation with MTA⁺ cation, which provides beneficial features to the sorption process. Aside from expanding the interlayer and basal spacing, the intercalation of MTA⁺ cation would expose additional charge-bearing sites for the binding of incoming amoxicillin or ampicillin molecules. The intercalated MTA⁺ cation would interact hydrophobically with amoxicillin or ampicillin through intermolecular attraction forces, possibly van der Waals force or permanent dipole-dipole interaction between positively charged nitrogen atom located at the ‘head’ of MTA⁺ cation and negatively charged carboxylate anion (RCOO⁻) in amoxicillin or ampicillin structure. The forces of electrostatic attraction acting between carboxylate anionic groups and positively charged clay’ edge

sites might also take place. Furthermore, the hydrophobic alkyl chain of the intercalated surfactant played important role by serving as a sorption domain for the allocation of organic (antibiotic) molecules.^{35–37} Thus, it can be argued that the intercalated surfactant cation in the clay’ interlayer spacing has a crucial influence by forming organic partition phases with quite different affinities toward the organic groups. Ultimately, there was no linear relation between the surface properties and adsorption capacity as O-MMT sorbent exhibited higher sorption capacity although its specific surface area and pore volume were lower compared to the original material.

Modeling adsorption isotherm data for single antibiotic systems

The so-called adsorption isotherm is vital information describing the equilibrium distribution of solute adsorbed on a solid surface to that of in the liquid with which it is in contact at a given temperature. The single component adsorption isotherms of amoxicillin and ampicillin were analyzed by Freundlich and Langmuir models. The Freundlich model, which originally developed in 1909 for expressing the isothermal variation of a quantity of gas adsorbed by unit mass of adsorbent with pressure, has an empirical mathematical form as follows:³⁸

$$q_e = K_F \times C_e^{1/n} \quad (3)$$

where K_F is the Freundlich constant related to the adsorption affinity [(mg g⁻¹) (L mg⁻¹)^{1/n} or (mmol g⁻¹) (L mmol⁻¹)^{1/n}] and n is a dimensionless intensity factor characterizing the surface heterogeneity degree. Generally, the value of constant n is greater than unity and the adsorption favorability can be evaluated based on the following n values: favorable (2–10), moderately difficult (1–2) and poor (<1).³⁹

Langmuir model is perhaps the simplest and most useful semi-empirical model for interpreting various physical and chemical adsorption phenomena in gas- and liquid-phase systems as well as many real sorption processes. Langmuir (1918) postulated his isotherm based on the kinetic principle of adsorption of gases on the plane surfaces of ideal solids.⁴⁰ The

mathematical expression of Langmuir isotherm is equated by the following formula:

$$q_e = q_m \frac{K_L C_e}{1 + K_L C_e} \quad (4)$$

where q_m is the Langmuir constant of maximum sorption capacity when the solid is covered with a monolayer (mg g^{-1} or mmol g^{-1}), also denotes a practical limiting sorption capacity and assists in the comparison of adsorption performance and K_L is the adsorption affinity constant (L mg^{-1} or L mmol^{-1}). The essential features of Langmuir isotherm can be expressed in terms of equilibrium parameter R_L , with classifications of the adsorption nature: favorable – convex isotherms ($0 < R_L < 1$), unfavorable–concave isotherms ($R_L > 1$), linear ($R_L = 1$) or highly favorable/non-reversible ($R_L = 0$). The R_L value can be calculated using a formula proposed by Weber and Chakravorti:⁴¹

$$R_L = \frac{1}{1 + K_L C_0} \quad (5)$$

where C_0 is the initial solute concentration in the liquid phase, which is 0.80 mmol L^{-1} for amoxicillin and 0.82 mmol L^{-1} for ampicillin.

The correlations of adsorption equilibrium data were performed by nonlinear regression fitting using SigmaPlot software (Version 12.3, Systat Software Inc.). Fig. 3 displays the fitting comparison between Freundlich and Langmuir models against single adsorption equilibrium data of amoxicillin and ampicillin. The values of the fitted isotherm parameters are listed in Table 2. At a glance, Langmuir isotherm describes experimental data better than Freundlich isotherm. The favorability of Langmuir model also visually confirmed from the isotherm curves that exhibit a convex character. According to system of classification of solution adsorption isotherms suggested by Giles and colleagues,⁴² the isotherm curves at all temperatures belong to a L2-type, which the indicative of solute adsorbed flat on the surface. Similar isotherm type was found for the immobilization of tetracycline on kaolinite surface¹⁸ and adsorption of an antihistamine medicine (chlorpheniramine) using Ca-montmorillonite²¹ and activated charcoal.⁴³

Considering the adsorption affinity, this parameter can rise or fall with temperature change, depending on whether physisorption or chemisorption that dominates in the sorption system. In this study where chemisorption controls the adsorption of amoxicillin and ampicillin, the adsorption affinity should be higher with increasing temperature because higher temperature hastens the movement of solute molecules in the liquid phase to be bound on the surface. Both Freundlich and Langmuir isotherms clarify this behavior, as shown in Table 2. Higher affinity of solute molecules to O-MMT surface is expected because the sorbent possesses organophilic surface stemming from the substitution of MTA^+ cation in place of interlayer Na^+ cation. In terms of adsorptivity, ampicillin was preferentially adsorbed to the surface rather than amoxicillin.

The next examination is on the parameter q_m of Langmuir model, which the indicative of maximum monolayer capacity of a particular sorbent. With the increase of temperature from 303.15 K to 323.15 K , the maximum monolayer capacity rose

from $0.079 \text{ mmol g}^{-1}$ to $0.090 \text{ mmol g}^{-1}$ for Na-MMT and from $0.143 \text{ mmol g}^{-1}$ to $0.157 \text{ mmol g}^{-1}$ for O-MMT if ampicillin was considered as the solute. The increasing maximum monolayer capacity accompanying temperature rise revealed that chemisorption was the controlling phenomenon. The remaining analysis is on the parameter n of Freundlich model, which is a characteristic constant for the surface heterogeneity degree. It can be seen that there is no clear correlation between this parameter and temperature, as in the sorption systems of amoxicillin/Na-MMT and amoxicillin/O-MMT, the values of n decrease with temperature increase while in the ampicillin/O-MMT system, an opposite trend is obtained. Even, a fluctuating value of n with temperature was observed in the ampicillin/Na-MMT system. It should also be noted that the magnitude of constant n should be higher for the adsorption on the O-MMT surface. Again, the Freundlich isotherm cannot capture this well. Therefore, it can be concluded that Langmuir isotherm outperforms Freundlich isotherm in describing adsorption equilibria data. In addition, the calculated R_L values all confirmed the favorable nature of adsorption process across the studied temperatures.

The adsorption capacity of O-MMT was compared with other adsorbents to evaluate its application as a viable alternative to treat amoxicillin and ampicillin from water and wastewater. Based on the Langmuir analysis, the maximum adsorption capacity of O-MMT was estimated to be $0.124\text{--}0.133 \text{ mmol g}^{-1}$ ($45.3\text{--}48.6 \text{ mg g}^{-1}$) for amoxicillin and $0.143\text{--}0.157 \text{ mmol g}^{-1}$ ($49.9\text{--}54.9 \text{ mg g}^{-1}$) for ampicillin. A number of studies had used activated carbons as the primary adsorbent to remove various antibiotics. Ding and co-workers⁴⁴ prepared the sludge-derived activated carbons to remove a mixture of 11 antibiotics include amoxicillin from diluted water solutions. The estimated total adsorption capacity of $80\text{--}300 \text{ mg g}^{-1}$ was obtained from the Langmuir–Freundlich prediction. Similar adsorption capacity of bare and NH_4Cl -induced activated carbons (261.8 vs. 438.6 mg g^{-1}) was reported by Moussavi *et al.*³² for batch adsorption of amoxicillin. Although the synthesized O-MMT exhibited lower uptake capacity than carbon-based materials, the preparation method of the organoclay is simpler and less energy- and time-consuming compared to chemical or thermal activation pathways to synthesize the carbons. Furthermore, the montmorillonite lump used to prepare the organoclay is a cheap and easily available material in large quantity. The application of organo-bentonite to remove amoxicillin had been investigated by Zha and colleagues.⁴⁵ However, lower adsorption capacity of the organobentonite ($27.85\text{--}30.12 \text{ mg g}^{-1}$ at 303.15 K and 313.15 K) was obtained compared to the values reported in this study. The O-MMT sorbent also showed superior adsorption capacity than chitosan beads⁴⁶ (45.3 vs. 8.71 mg g^{-1} at pH 6.5) for batch amoxicillin removal.

Modeling adsorption isotherm data for binary antibiotic systems

Multicomponent adsorption depends on the number of solutes competing for the sorption sites, their speciation,

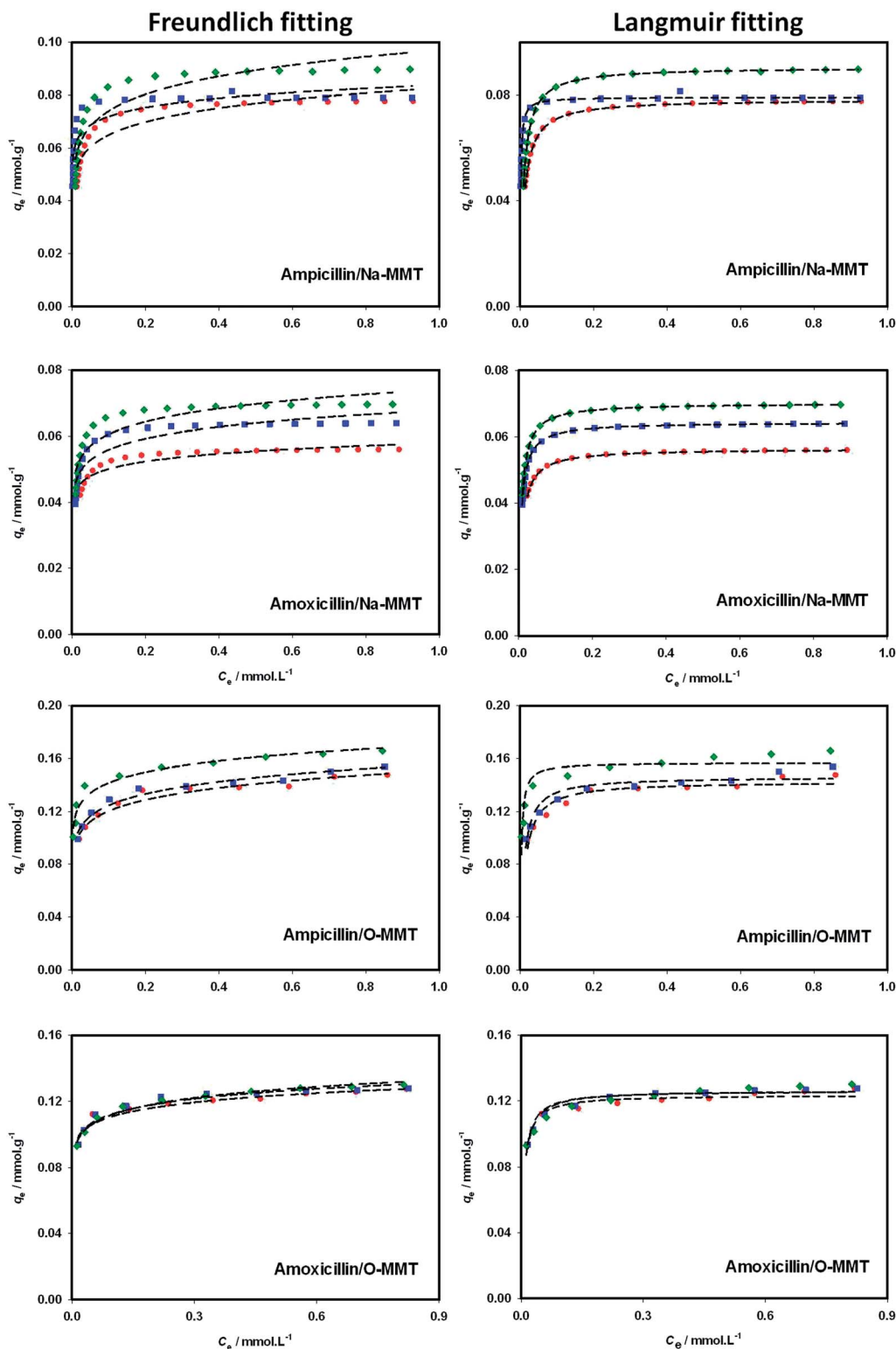


Fig. 3 The Freundlich and Langmuir model fittings against single adsorption equilibrium data of amoxicillin and ampicillin (● 303.15 K, ■ 313.15 K and ◆ 323.15 K).

concentrations, residence time, *etc.*, which all contribute to the interference and competition phenomena in the solution and at the solid/solution interface.⁴⁷ Often, most of available empirical or semi-empirical models lack of theoretical basis

and they may not be able to accurately analyze the system behavior over the entire range of measurements. Notwithstanding the most realistic model so-called the ideal adsorption solution theory (IAST) and its modifications, such

Table 2 Correlation isotherm parameters for adsorption of amoxicillin and ampicillin in single component systems as fitted with Freundlich and Langmuir models

Adsorbent	Adsorbate	<i>T</i> (K)	Freundlich parameters			Langmuir parameters			
			K_F (mmol g ⁻¹) (L mmol ⁻¹) ^{-<i>n</i>}	<i>n</i>	<i>R</i> ²	<i>q</i> _m (mmol g ⁻¹)	<i>K</i> _L (L mmol ⁻¹)	<i>R</i> ²	<i>R</i> _L
Na-MMT	Ampicillin	303.15	0.083	9.54	0.87	0.079	124.81	0.99	0.0092
		313.15	0.089	15.12	0.82	0.080	158.09	0.98	0.0073
		323.15	0.097	8.51	0.86	0.090	169.56	0.98	0.0068
	Amoxicillin	303.15	0.058	15.86	0.86	0.056	96.68	0.99	0.0124
		313.15	0.068	13.96	0.85	0.064	108.29	0.98	0.0111
		323.15	0.074	12.45	0.86	0.071	113.46	0.99	0.0106
O-MMT	Ampicillin	303.15	0.151	10.22	0.95	0.143	141.11	0.95	0.0082
		313.15	0.156	10.34	0.97	0.146	183.37	0.94	0.0063
		323.15	0.170	12.53	0.96	0.157	206.44	0.94	0.0056
	Amoxicillin	303.15	0.129	15.30	0.94	0.124	122.94	0.93	0.0098
		313.15	0.132	14.32	0.94	0.126	143.75	0.97	0.0084
		323.15	0.134	13.03	0.98	0.133	182.58	0.95	0.0066

as fast-IAS and real adsorption solution theory have found reasonable success to correlate multicomponent adsorption equilibria data, the complex algorithm for the model solution involving numerical integration at each step of iteration procedure requires the use of advanced computer resources. On the other hand, extended-Langmuir is a simple model with adequate thermodynamic basis and useful insights for analyzing multicomponent adsorption equilibria. To describe the equilibrium competitive adsorption in the multicomponent systems, Langmuir model for pure component adsorption equilibria can be easily extended to the following formulation:

$$q_{e,i} = \frac{q_{m,i} K_{L,i} C_{e,i}}{1 + \sum_{i=1}^N K_{L,i} C_{e,i}} \quad (6)$$

where *i* is the number of components, *q*_{m,*i*} and *q*_{e,*i*} are the maximum adsorbed amount of each component (mmol g⁻¹) and the adsorbed amount of each component per mass of adsorbent at equilibrium concentration *C*_{e,*i*} and *K*_{L,*i*} is the individual adsorption affinity constant of each component (L mmol⁻¹). For a liquid phase system consisting of two components, one can use the extended-Langmuir equation in the form:

$$q_{e,1} = \frac{q_{m,1} K_{L,1} C_{e,1}}{1 + K_{L,1} C_{e,1} + K_{L,2} C_{e,2}} \quad (7)$$

$$q_{e,2} = \frac{q_{m,2} K_{L,2} C_{e,2}}{1 + K_{L,1} C_{e,1} + K_{L,2} C_{e,2}} \quad (8)$$

The success of the extended-Langmuir model in analyzing binary adsorption equilibrium data has been reported in several studies.^{47–49} The validity of the model was justified based on the simple error minimization between predicted and measured *q*_e values. The predicted *q*_e values for each component can be calculated from eqn (7) and (8) by introducing the fitted parameters *q*_m and *K*_L belonging to single adsorption data. Such approach, however, does not fit for correlating binary

adsorption data because adsorption in the binary system involves interference and competition between solutes in the solution and on the active surface sites; both these characteristics are negated in the single adsorption system. Therefore, to improve the accuracy of predictions and theoretical sound of the extended-Langmuir model, we propose a modification to each parameter above by addressing competitive adsorption behavior.

In the binary system, the active sorption sites are accommodated by two solutes with a specific surface coverage. Therefore, the maximum sorption capacity should be the sum of fraction of surface covered by each solute multiplied by its maximum sorption capacity or can be expressed as follows:

$$q_{m,\text{bin}} = q_{m,1(\text{singl})}\theta_1 + q_{m,2(\text{singl})}\theta_2 \quad (9)$$

where θ_1 and θ_2 are the fractional surface coverage of solute 1 and 2, respectively. Here, we argue that total monolayer surface coverage by both solutes should not exceed unity, considering that some surface sites are inactive for adsorption. The parameter *K*_L measures how strong the solute molecules are attracted to the surface. The higher the affinity, the more solute molecules are adsorbed on the surface. Since the solute species compete each other, their affinities to the surface should be weaker compared to that of single adsorption system. Accordingly, the use of parameter *K*_L from single adsorption data is not valid and a simple theoretical treatment to this parameter is given as follows:

$$K_{L,1(\text{bin})} = K_{L,1(\text{singl})} \left(1 - \frac{\theta_2}{\theta_1 + \theta_2} \right) \quad (10)$$

$$K_{L,2(\text{bin})} = K_{L,2(\text{singl})} \left(1 - \frac{\theta_1}{\theta_1 + \theta_2} \right) \quad (11)$$

In eqn (10) and (11), the competitive adsorption between solutes is expressed as a ratio of fraction of surface covered by one solute to that of total surface coverage by both solutes.

Introducing eqn (10) and (11) into eqn (7) and (8) gives the following equations:

$$q_{e,1(\text{bin})} = \frac{(q_{m,1(\text{singl})}\theta_1 + q_{m,2(\text{singl})}\theta_2)K_{L,1(\text{singl})}\left(1 - \frac{\theta_2}{\theta_1 + \theta_2}\right)C_{e,1(\text{bin})}}{1 + K_{L,1(\text{singl})}\left(1 - \frac{\theta_2}{\theta_1 + \theta_2}\right)C_{e,1(\text{bin})} + K_{L,2(\text{singl})}\left(1 - \frac{\theta_1}{\theta_1 + \theta_2}\right)C_{e,2(\text{bin})}} \quad (12)$$

$$q_{e,2(\text{bin})} = \frac{(q_{m,1(\text{singl})}\theta_1 + q_{m,2(\text{singl})}\theta_2)K_{L,2(\text{singl})}\left(1 - \frac{\theta_1}{\theta_1 + \theta_2}\right)C_{e,2(\text{bin})}}{1 + K_{L,1(\text{singl})}\left(1 - \frac{\theta_2}{\theta_1 + \theta_2}\right)C_{e,1(\text{bin})} + K_{L,2(\text{singl})}\left(1 - \frac{\theta_1}{\theta_1 + \theta_2}\right)C_{e,2(\text{bin})}} \quad (13)$$

Eqn (12) and (13) are both called as the modified extended-Langmuir model. Here, θ_1 and θ_2 were treated as fitting parameters with the following constraints: $\theta_1 > 0$, $\theta_2 > 0$ and $\theta_1 + \theta_2 < 1$. The proposed model was fitted to experimental data by performing computer-aided nonlinear regression fitting. The accuracy of predictions was assessed from the coefficient of determination (R^2) values obtained from the computational results.

The binary adsorption equilibrium data are obtained by conducting adsorption experiments at 303.15 K and near-neutral pH with O-MMT as the sorbent and mixtures of amoxicillin and ampicillin as the waste effluents. Here, O-MMT was employed as the sorbent due to its superior adsorption capacity compared to Na-MMT. Also, the choice of conducting binary adsorption experiments at pH range of 6–7 was based on the single adsorption results in which at this pH range, the highest removal of amoxicillin and ampicillin took place. Fig. 4 shows the correlation results of binary adsorption equilibrium data fitted with the modified extended-Langmuir model (represented as wire-mesh plot). The values of θ_1 and θ_2 obtained from the model fitting are given in Table 3. From Fig. 4, it can be seen that the modified extended-Langmuir model can correlate binary adsorption data adequately. In comparison, the fitness of original extended-Langmuir model to the experimental data is given in the ESI Fig. S7.† Noticeably, the modified extended-Langmuir model gave better representation than the original model, suggesting that the inclusion of fractional surface coverage may improve the accuracy of predictions and assist in interpreting the adsorption behavior in binary system. The fraction of active sorption sites covered by either amoxicillin or ampicillin decreases as the concentration of the opposite adsorbate in the mixture increased. For example, the fraction of adsorption sites covered by amoxicillin for effluent A (75 wt% amoxicillin + 25 wt% ampicillin) was 0.639 and this value

decreased to 0.437 and 0.263 with increasing ampicillin concentration to 50 wt% and 75 wt%, respectively. Likewise, the

ampicillin loading on the surface of O-MMT increased with decreasing concentration of amoxicillin in the mixture. One can also notice that total monolayer coverage on the surface in all systems is similar, typically about 0.89 (expressed as a fractional quantity). This supports our previous argument that some of the surface sites are unavailable for the sorption, likely due to the surfactant blockade and to consider that the sorbent has a void fraction. With regard to adsorptivity, both amoxicillin and ampicillin are less likely adsorbed on the surface due to competition effect. Consequently, fewer amounts of amoxicillin (44.8%) and ampicillin (48.3%) were removed from a binary mixture (effluent B) compared to single solute systems for near-neutral pH adsorption. To this end, the modified extended-Langmuir model will turn back into the original Langmuir model if only one solute component is considered in the sorption system (θ_2 and $C_{e,2}$ are zero in eqn (12) and θ_1 and $C_{e,1}$ are zero in eqn (13)).

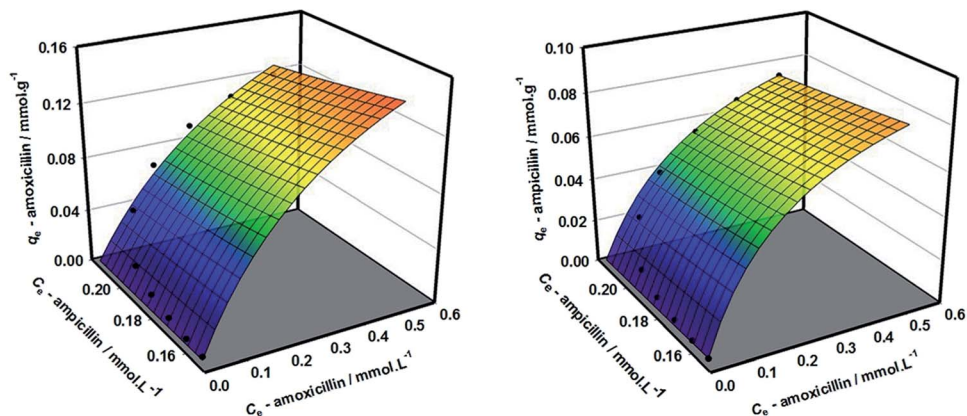
Adsorption thermodynamic

Adsorption thermodynamic relates the equilibrium of adsorption to those properties which cannot be directly measured from the experiment, such as activation energy (E_a , kJ mol⁻¹), the Gibb's free energy change (ΔG° , kJ mol⁻¹), standard enthalpy change (ΔH° , kJ mol⁻¹), standard entropy change (ΔS° , kJ mol⁻¹ K⁻¹) and isosteric heat of adsorption (ΔH_{st} , kJ mol⁻¹). The Gibb's free energy change is an important criterion for spontaneity of a chemical process and it can be related to adsorption equilibrium constant by the following reaction isotherm:

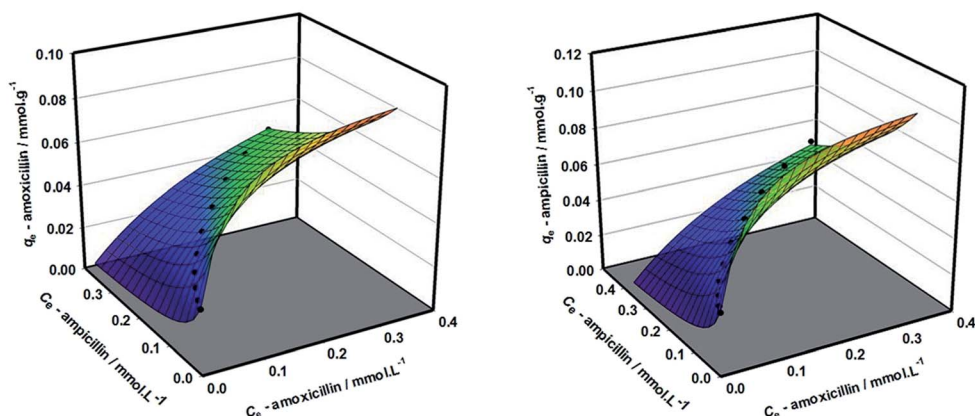
$$\Delta G^\circ = -RT \ln K_D \quad (14)$$

where R is the ideal gas constant (8.314 J mol⁻¹ K⁻¹), T is the temperature (K) and K_D is the linear sorption distribution

Effluent A (75 wt.% amoxicillin + 25 wt.% ampicillin)



Effluent B (50 wt.% amoxicillin + 50 wt.% ampicillin)



Effluent C (25 wt.% amoxicillin + 75 wt.% ampicillin)

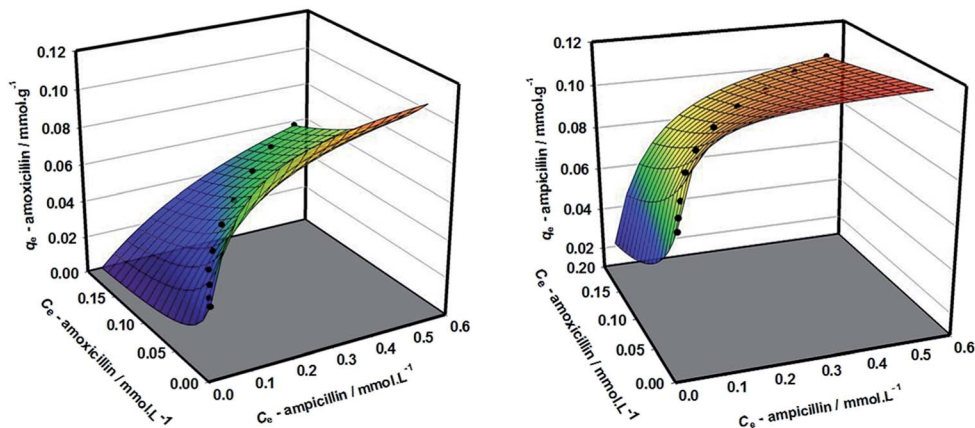


Fig. 4 The fitting performance of modified extended-Langmuir model against binary adsorption equilibrium data of various effluents containing amoxicillin and ampicillin.

coefficient, defined as a ratio between the equilibrium surface concentration of adsorbed solute and the equilibrium solute concentration in the liquid phase. The value of K_D is determined by plotting a straight line of $\ln(q_e/C_e)$ versus C_e and extrapolating to zero C_e according to Khan and Singh.⁵⁰ The variation of thermodynamic equilibrium constant with temperature can be expressed in terms of standard enthalpy change and standard entropy change by the classical van't Hoff formula:

$$\ln K_D = \frac{\Delta S^0}{R} - \frac{\Delta H^0}{RT} \quad (15)$$

A plot of natural logarithm of the thermodynamic equilibrium constant, $\ln K_D$ versus the reciprocal temperature, $1/T$ (Fig. 5) will be linear with the slope and y-intersection point giving the values of ΔH^0 and ΔS^0 , respectively.

Table 3 The fitted and calculated equilibrium parameters for binary adsorption of effluents containing amoxicillin (adsorbate 1) and ampicillin (adsorbate 2)^a

Effluents	Fitted parameters		Calculated parameters			R^2
	θ_1	θ_2	$K_{L,1(\text{bin})}$ (L mmol ⁻¹)	$K_{L,2(\text{bin})}$ (L mmol ⁻¹)	$q_{m,\text{bin}}$ (mmol g ⁻¹)	
A	0.639	0.253	88.07	40.02	0.115	0.97
B	0.437	0.455	60.23	71.98	0.119	0.98
C	0.263	0.618	36.70	98.98	0.121	0.98

^a Adsorption temperature = 303.15 K, Adsorbent = O-MMT.

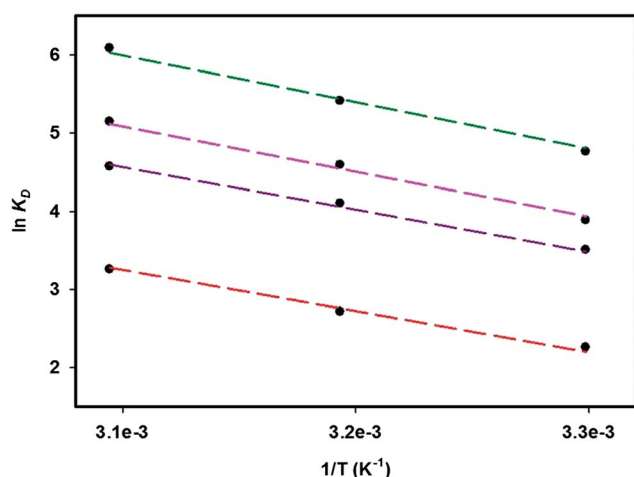


Fig. 5 Thermodynamic plots of $\ln K_D$ versus $1/T$ for the adsorption of amoxicillin and ampicillin in single component systems (— — — amoxicillin/Na-MMT; — — — ampicillin/Na-MMT; — — — amoxicillin/O-MMT; — — — ampicillin/O-MMT).

Table 4 summarizes the values of thermodynamic parameters for single adsorption of amoxicillin and ampicillin. The free energy change of adsorption decreased with an increase in temperature and this suggests that higher temperature makes the sorption process easier. The negative values of ΔG° confirm that adsorption is thermodynamically feasible and spontaneous with high preference of solutes to the surface. In this case, the adsorption of amoxicillin and ampicillin on O-MMT is more likely to take place at a given temperature, as reflected from the

magnitude of ΔG° values. The values of ΔH° and ΔS° are 43.8 kJ mol⁻¹ and 162.8 J mol⁻¹ K⁻¹ for amoxicillin/Na-MMT system and 45.3 kJ mol⁻¹ and 178.4 J mol⁻¹ K⁻¹ for ampicillin/Na-MMT system. The positive sign of ΔH° is an indication of the endothermicity of adsorption and suggests the possibility of strong binding between adsorbate and adsorbent. Furthermore, the magnitude of ΔH° values may give an idea whether the adsorption belongs to physisorption (2.1–20.9 kJ mol⁻¹) or chemisorption (80–200 kJ mol⁻¹). As shown in Table 4, it seems that the adsorption of amoxicillin and ampicillin on Na-MMT or O-MMT can be attributed to the combination of physisorption and chemisorption rather than a pure physical or chemical adsorption.

The thermodynamic quantity ΔS° is defined as a measure of randomness in the system. The positive value of ΔS° reflects high affinity of solute to the sorption sites, also the increased randomness at the solid/solution interface during adsorption process. Some significant changes in the internal structure of adsorbate and adsorbent may cause the system to gain extra translational and rotational entropies, such as from the displacement of adsorbed water by the adsorbate, interlayer cation exchange between Na⁺ and MTA⁺ or the partitioning of adsorbate species in the hydrophobic alkyl chain of the intercalated surfactant. Furthermore, the positive value of ΔS° revealed a strong confinement of solute in the solid phase. Since binary adsorption experiments in this study were conducted at single temperature (303.15 K), it is not possible to analyze thermodynamic behavior of the process. However, one can predict it theoretically, for instance the values of free energy change of adsorption should be less negative because adsorption is less energetically favorable. Also, the magnitude of the entropy change might be greater due to increased disorder in the system as a result of competitive adsorption between the adsorbed components.

Batch adsorption tests using real pharmaceutical wastewater and regenerability evaluation

In order to test the feasibility of O-MMT adsorbent for real sorption application, batch adsorption experiments using real pharmaceutical wastewater were conducted at 303.15 K for 24 h. The adsorbent dose was fixed at 10 g L⁻¹. The wastewater was randomly collected from five sampling points from a wastewater treatment plant of local pharmaceutical and health care products manufacturer at Sidoarjo city, East Java. Prior to

Table 4 Thermodynamic parameters for adsorption of amoxicillin and ampicillin in single component systems

Adsorbents	T (K)	Amoxicillin			Ampicillin		
		ΔG° (kJ mol ⁻¹)	ΔS° (J mol ⁻¹ K ⁻¹)	ΔH° (kJ mol ⁻¹)	ΔG° (kJ mol ⁻¹)	ΔS° (J mol ⁻¹ K ⁻¹)	ΔH° (kJ mol ⁻¹)
Na-MMT	303.15	-5.55	162.8	43.8	-8.78	178.4	45.3
	313.15	-7.18			-10.56		
	323.15	-8.81			-12.35		
O-MMT	303.15	-9.92	191.4	48.1	-12.12	203.6	49.6
	313.15	-11.84			-14.16		
	323.15	-13.75			-16.19		

adsorption, the collected samples were vacuum-filtered with a Buchner funnel to remove coarse particles. The initial pH of the wastewater ranged between 5.5 and 6. Amoxicillin and ampicillin were detected as two major constituents with initial concentrations of 0.16 and 0.11 mmol L⁻¹, respectively. Other antibiotics, such as ciprofloxacin, chloramphenicol and cefotaxime were also detected in trace levels (Table S4 in the ESI†).

Solution of 0.1 M CaCl₂ was used as the desorbing agent. Desorption experiments were carried out by mixing antibiotics-loaded O-MMT sorbent with CaCl₂ (solution to solid ratio of 100) and the mixture was allowed to stand for 24 h under shaking at room temperature. The removal percentages of each antibiotic as a function of regeneration cycle are displayed in Fig. 6. The highest removal percentage was observed for amoxicillin, followed by ampicillin, chloramphenicol, ciprofloxacin and cefotaxime with total removal percentage of 68.2%. A gradual decrease in the removal percentage of each antibiotic was noticed as the regeneration cycles progressed; likely due to the inability of desorbing solution to completely detach bound antibiotics from the organoclay surface. Similar observation was obtained by Wu *et al.*⁵¹ for desorption studies of ciprofloxacin from kaolinite and montmorillonite clays. By the end of the fifth cycle, total removal percentage of all antibiotics by O-MMT was 49.5%. These results show that O-MMT is a promising sorbent for economical and effective treatment of real effluents containing antibiotic compounds. Furthermore, O-MMT sorbent possesses good adsorptive retention since total removal percentage was about 50% even after five successive adsorption–desorption cycles. Desorption of antibiotics from the organoclay surface might be due to the ligand-promoted dissolution of metal-antibiotic surface complexes between Ca²⁺ and the zwitterionized antibiotics through the involvement of carboxylic (–COO⁻) groups.^{51,52} FT-IR spectroscopy study of O-MMT sorbent after desorption by CaCl₂ solution (see Fig. S3 in the ESI†) supported this argument in which the intensities of absorption peaks associated with C=O stretching of carboxylic

group at ~1700 cm⁻¹ and N–H stretching and bending vibrations of amine group at ~3400 cm⁻¹ and ~1600 cm⁻¹ diminished. In addition, the stretching peaks correspond to sp³ C–H bond in CH₃ and CH₂ groups at 2900–2800 cm⁻¹ remain unaltered after Ca²⁺ desorption, indicating that cation exchange between MTA⁺ in the interlayer spacing and Ca²⁺ was not feasible to take place, due to the latter cation possesses lower affinity than the former toward the clay surface.

Conclusions

Organo-montmorillonite (O-MMT) with high adsorption capacity and organophilic surface has been successfully prepared by microwave-assisted irradiation of aqueous suspension containing Na-montmorillonite (Na-MMT) and MTAB cationic surfactant. The synthesized O-MMT showed potential applications for detoxifying amoxicillin and ampicillin in single and binary systems. Analysis of adsorption equilibrium data for single antibiotic systems revealed that Langmuir model outperformed Freundlich model. The proposed extended-Langmuir model with the inclusion of surface coverage was superior to original model in representing binary adsorption equilibrium data. The proposed model can also adequately capture theoretical insights of binary sorption behavior. Thermodynamically, the adsorption of amoxicillin and ampicillin on Na-MMT/O-MMT was energetically favorable/spontaneous ($\Delta G^\circ < 0$) and endothermic ($\Delta H^\circ > 0$) with high preference of adsorbed solutes toward the surface ($\Delta S^\circ > 0$). The regeneration study revealed the feasibility of O-MMT sorbent to be efficiently reused for five cycles of adsorption–desorption in handling real pharmaceutical wastewater containing multiple antibiotic compounds.

References

- 1 R. N. Brogden, A. Carmine, R. C. Heel, P. A. Morley, T. M. Speight and G. S. Avery, *Drugs*, 1981, **22**, 337–362.
- 2 J. P. Hou and J. W. Poole, *J. Pharm. Sci.*, 1971, **60**, 503–532.
- 3 H. Schmitt and J. Rombke, in *Pharmaceuticals in the Environment: Sources, Fate, Effects and Risks*, ed. K. Kummerer, Springer Berlin Heidelberg, Berlin, 2008, pp. 285–303.
- 4 M. V. Walter and J. W. Vennes, *Appl. Environ. Microbiol.*, 1985, **50**, 930–933.
- 5 L. Guardabassi, D. M. A. Lo Fo Wong and A. Dalsgaard, *Water Res.*, 2002, **36**, 1955–1964.
- 6 M. L. Richardson and J. M. Bowron, *J. Pharm. Pharmacol.*, 1985, **37**, 1–12.
- 7 T. Coskun, H. A. Kabuk, K. B. Varınca, E. Debik, I. Durak and C. Kavurt, *Bioresour. Technol.*, 2012, **121**, 31–35.
- 8 S. Larcher and V. Yargeau, *Appl. Microbiol. Biotechnol.*, 2012, **96**, 309–318.
- 9 R. Andreozzi, M. Canterino, R. Marotta and N. Paxeus, *J. Hazard. Mater.*, 2005, **122**, 243–250.
- 10 I. A. Balcioglu and M. Otker, *Chemosphere*, 2003, **50**, 85–95.
- 11 K. A. Rickman and S. P. Mezyk, *Chemosphere*, 2010, **81**, 359–365.

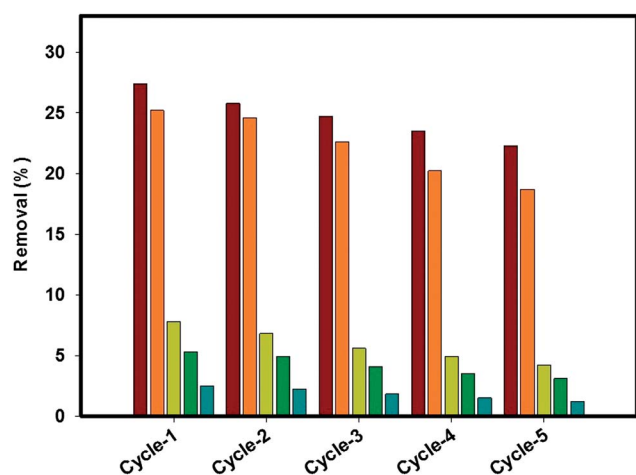


Fig. 6 Removal percentages of various antibiotics in real pharmaceutical effluents and reusability tests of O-MMT adsorbent (■ amoxicillin; ■ ampicillin; ■ chloramphenicol; ■ ciprofloxacin; ■ cefotaxime).

- 12 S. Z. Li, X. Y. Li and D. Z. Wang, *Sep. Purif. Technol.*, 2004, **34**, 109–114.
- 13 Z. Qiang, J. J. Macauley, M. R. Mormile, R. Surampalli and C. D. Adams, *J. Agric. Food Chem.*, 2006, **54**, 8144–8154.
- 14 E. S. Elmolla and M. Chaudhuri, *J. Hazard. Mater.*, 2010, **173**, 445–449.
- 15 E. S. Elmolla and M. Chaudhuri, *Desalination*, 2011, **272**, 218–224.
- 16 X. Xiao, R. P. Hu, C. Liu, C. L. Xing, X. X. Zuo, J. M. Nan and L. S. Wang, *Chem. Eng. J.*, 2013, **225**, 790–797.
- 17 M. Miyata, I. Ihara, G. Yoshida, K. Toyod and K. Umetsu, *Water Sci. Technol.*, 2011, **63**, 456–461.
- 18 Z. H. Li, L. Schulz, C. Ackley and N. Fenske, *J. Colloid Interface Sci.*, 2010, **351**, 254–260.
- 19 W. Yan, J. F. Zhang and C. Y. Jing, *J. Colloid Interface Sci.*, 2013, **390**, 196–203.
- 20 N. Liu, M. x. Wang, M. m. Liu, F. Liu, L. P. Weng, L. K. Koopal and W. f. Tan, *J. Hazard. Mater.*, 2012, **225–226**, 28–35.
- 21 Z. H. Li, P. H. Chang, J. S. Jean, W. T. Jiang and H. L. Hong, *Colloids Surf., A*, 2011, **385**, 213–218.
- 22 S. M. Mitchell, J. L. Ullman, A. L. Teel and R. J. Watts, *Sci. Total Environ.*, 2014, **466–467**, 547–555.
- 23 H. Xu, W. J. Cooper, J. Jung and W. Song, *Water Res.*, 2011, **45**, 632–638.
- 24 S. J. Chipera, G. D. Guthrie and D. L. Bish, *Rev. Mineral. Geochem.*, 1993, **28**, 235–249.
- 25 Y. Yang, Y. Chun, G. Y. Sheng and M. S. Huang, *Langmuir*, 2004, **20**, 6736–6741.
- 26 P. L. Ravikovitch and A. V. Neimark, *Langmuir*, 2000, **16**, 2419–2423.
- 27 H. He, R. L. Frost, T. Bostrom, P. Yuan, L. Duong, D. Yang, Y. Xi and J. T. Klopogge, *Appl. Clay Sci.*, 2006, **31**, 262–271.
- 28 H. He, Y. Ma, J. Zhu, P. Yuan and Y. Qing, *Appl. Clay Sci.*, 2010, **48**, 67–72.
- 29 H. He, Q. Zhou, W. N. Martens, T. J. Klopogge, P. Yuan, Y. Xi, J. Zhu and R. L. Frost, *Clays Clay Miner.*, 2006, **54**, 689–696.
- 30 H. He, D. Yang, P. Yuan, W. Shen and R. L. Frost, *J. Colloid Interface Sci.*, 2006, **297**, 235–243.
- 31 J. H. Choy, S. Y. Kwak, Y. S. Han and B. W. Kim, *Mater. Lett.*, 1997, **33**, 143–147.
- 32 G. Moussavi, A. Alahabadi, K. Yaghmaeian and M. Eskandari, *Chem. Eng. J.*, 2013, **217**, 119–128.
- 33 W. T. Jiang, P. H. Chang, Y. S. Wang, Y. Tsai, J. S. Jean, Z. Li and K. Krukowski, *J. Hazard. Mater.*, 2013, **250–251**, 362–369.
- 34 C. J. Wang, Z. Li, W. T. Jiang, J. S. Jean and C. C. Liu, *J. Hazard. Mater.*, 2010, **183**, 309–314.
- 35 L. Zhu and R. Zhu, *Colloids Surf., A*, 2008, **320**, 19–24.
- 36 T. Wang, J. Zhu, R. Zhu, F. Ge, P. Yuan and H. He, *J. Hazard. Mater.*, 2010, **178**, 1078–1084.
- 37 R. Zhu, L. Zhu, J. Zhu and L. Xu, *Sep. Purif. Technol.*, 2008, **63**, 156–162.
- 38 H. M. F. Freundlich, *Z. Phys. Chem.*, 1906, **57(A)**, 385–470.
- 39 O. Hamdaoui, *J. Hazard. Mater.*, 2006, **135**, 264–273.
- 40 I. Langmuir, *J. Am. Chem. Soc.*, 1918, **40**, 1361–1403.
- 41 T. W. Weber and R. K. Chakravorty, *AIChE J.*, 1974, **20**, 228–238.
- 42 C. H. Giles, T. H. MacEwan, S. N. Nakhwa and D. Smith, *J. Chem. Soc.*, 1960, **786**, 3973–3993.
- 43 D. O. Cooney, *Clin. Toxicol.*, 1995, **33**, 213–217.
- 44 R. Ding, P. Zhang, M. Seredych and T. J. Bandosz, *Water Res.*, 2012, **46**, 4081–4090.
- 45 S. X. Zha, Y. Zhou, X. Jin and Z. Chen, *J. Environ. Manage.*, 2013, **129**, 569–576.
- 46 W. S. Adriano, V. Veredas, C. C. Santana and L. R. B. Goncalves, *Biochem. Eng. J.*, 2005, **27**, 132–137.
- 47 K. K. H. Choy, J. F. Porter and G. McKay, *J. Chem. Eng. Data*, 2000, **45**, 575–584.
- 48 S. J. Allen, G. McKay and J. F. Porter, *J. Colloid Interface Sci.*, 2004, **280**, 322–333.
- 49 S. Al-Asheh, F. Banat, R. Al-Omari and Z. Duvnjak, *Chemosphere*, 2000, **41**, 659–665.
- 50 A. A. Khan and R. P. Singh, *Colloids Surf.*, 1987, **24**, 33–42.
- 51 Q. Wu, Z. Li, H. Hong, R. Li and W. T. Jiang, *Water Res.*, 2013, **47**, 259–268.
- 52 C. Gu and K. G. Karthikeyan, *Environ. Sci. Technol.*, 2005, **39**, 9166–9173.